The Astrophysical Journal, 982:145 (10pp), 2025 April 1 https://doi.org/10.3847/1538-4357/adba49

High-energy Jet Emission from GRS 1758–258 and 1E 1740.7–2942 with INTEGRAL?

James Rodi, Angela Bazzano, and Pietro Ubertini
INAF—Istituto di Astrofisica e Planetologia Spaziali, via Fosso del Cavaliere 100, 00133 Roma, Italy
Received 2024 November 9; revised 2025 February 20; accepted 2025 February 20; published 2025 March 26

Abstract

GRS 1758–258 and 1E 1740.7–2942 are two long-known persistent black hole binaries in the Galactic center region. Using the International Gamma-Ray Astrophysics Laboratory (INTEGRAL)'s extensive monitoring of the Galactic center and bulge, we studied their temporal and spectral evolutions in the 30–610 keV energy range from 2003 March through 2022 April with the Imager on Board INTEGRAL/INTEGRAL Soft Gamma-ray Imager gamma-ray telescope. Our analyses found that the sources typically had Comptonized spectra, though not always with the same parameters. The spectral states with more than 8 Ms of observation time show deviations from a Comptonized spectrum above ∼200 keV or a "hard tail" that extends up to at least 600 keV. The origin of this component remains debated, with the most popular scenarios being synchrotron emission from the jet or Comptonization in a hybrid thermal/nonthermal plasma. Anyway, the GRS 1758–258 and 1E 1740.7–2942 spectra are acceptably described by `CompTT+po` (jet) and `Eqpair` (hybrid Comptonization) scenarios. To differentiate between the two scenarios, we calculated the Spearman correlation coefficient comparing 30–50 keV count rates with those in higher energy bands (50–100, 100–300, and 300–600 keV). The count rates below 300 keV are strongly correlated, indicating those photons arise from the same physical process. Above 300 keV the count rates are either anticorrelated or not correlated with the 30–50 keV count rates for GRS 1758–258, which suggests that the photons originate from a different physical process. For 1E 1740.7–2942, the level of correlation is unclear due to scatter in the data points. However, the 300–600 keV count rates are consistent with a constant value. This disfavors the hybrid Comptonization scenario for both sources.

Unified Astronomy Thesaurus concepts: Low-mass x-ray binary stars (939); Gamma-ray astronomy (628)

1. Introduction

1E 1740.7–2942 (hereafter 1E) and GRS 1758–258 (GRS) are two of a handful of persistent, though variable, black hole binaries in the Galaxy. In particular, these two sources belong to the low-mass X-ray binary (LMXB) class and spend most of their time in the so-called hard state and part of the time in thermally dominated soft states and intermediate states. They are both observed at various energy bands and considered microquasars because of their radio characteristics, i.e., radio jets (L. F. Rodriguez et al. 1992; I. F. Mirabel & L. F. Rodríguez 1999) and double-lobed counterparts (J. Martí et al. 2017). The sources are located in a crowded field close to the Galactic center at a distance of 8 ± 1 kpc. For GRS the distance was estimated taking into account jet–interstellar medium interaction (A. J. Tetarenko et al. 2020).

The spectral and flux variability for 1E and GRS are similar and, being classified as LMXBs, accrete matter via Roche lobe overflow from the companion star. They are in general in the hard state and show few transitions into intermediate and dim states. For the hard state, spectra typically consist of a power-law component with a photon index around 1.6 and exponential cutoff <50–100 keV. The soft- and intermediate-state spectra are characterized by a disk component and a power law with photon index >2.

Several previous works have reported on relatively short INTEGRAL Soft Gamma-ray Imager (ISGRI) observations of GRS or 1E. For example, K. Pottschmidt et al. (2006) studied the hard to soft transition in 2003 and 2004 with RXTE/Proportional Counter Array (PCA) and ISGRI, while M. Del Santo et al. (2005) investigated the spectral variability of 1E during the same period, also with PCA and ISGRI. Later analyses of 1E by M. Castro et al. (2014) looked at spectral variability during brief periods in 2003, 2005, and 2012 with XMM-Newton, International Gamma-Ray Astrophysics Laboratory (INTEGRAL)/JEM-X, and ISGRI, and L. Natalucci et al. (2014) investigated the spectral and timing properties of 1E in the hard state with ISGRI and NuSTAR observations from 2012. Hereafter we report on the long-term characteristics of the two sources with high-energy broadband results from ISGRI.

2. Instruments and Observations

In 2002 October, the INTEGRAL satellite was launched from Baikonur, Kazakhstan (P. L. Jensen et al. 2003). The satellite is outside Earth's radiation belts for ∼85% of the 2.5–3 day orbit. We utilized the Imager on Board INTEGRAL (IBIS)/ISGRI (F. Lebrun et al. 2003; P. Ubertini et al. 2003) data in the 30–900 keV energy range.

GRS and 1E have been frequently monitored throughout the INTEGRAL mission with observations during Galactic center and bulge programs. The observations used in the subsequent analyses of GRS are within 10° of the spacecraft pointing direction during revolutions 46–2495 (MJD 52699–59693, 2003 March 1–2022 April 25 UTC). The same angular and temporal constraints were applied in selecting observations of 1E. This results in 18,422 pointings, or science windows (scws), for GRS and 18,457 scws for 1E, resulting in 26.00 Ms of total exposure time for GRS and 24.65 Ms of exposure time for 1E.

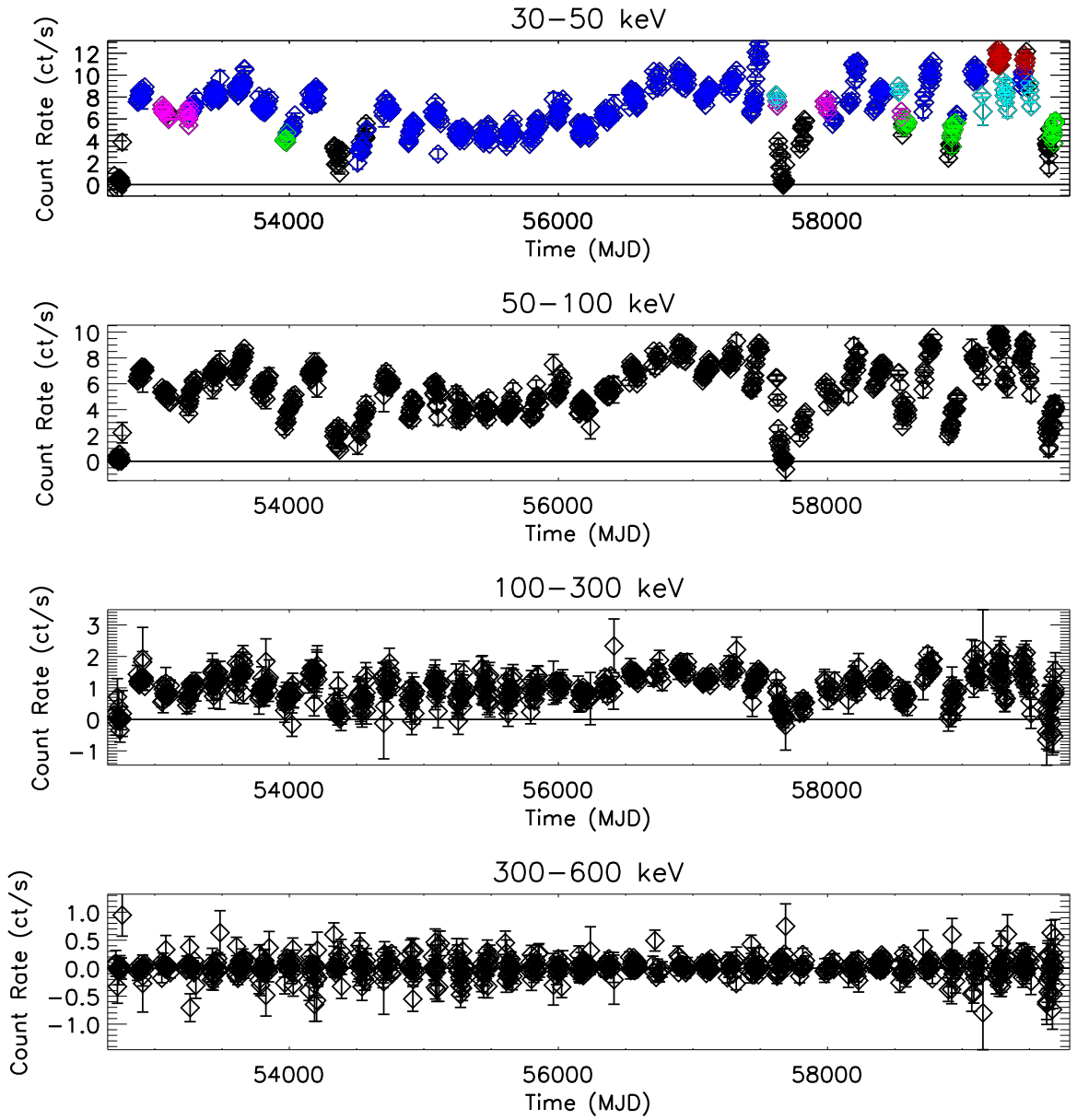

Figure 1. ISGRI long-term light curves of GRS in the 30–50, 50–100, 100–300, and 300–600 keV energy bands. Black solid line denotes 0 counts s^{-1}. The different colors in the 30–50 keV light curve correspond to different spectral states discussed in Section 3.2.1.

Data reduction was performed using the standard INTEGRAL Offline Science Analysis software version 11.2. The light-curve analysis was performed in five energy bins from 30–900 keV, while the spectral analysis used 62 energy bins in the same energy range. A systematic error of 1.5% was added to the spectral fitting.

3. Results

3.1. Temporal Variability

3.1.1. GRS 1758–258

As discussed above, GRS is a persistent source at hard X-rays/soft gamma rays. Figure 1 shows the ISGRI light curves on a revolution timescale (∼2.5–3 days) in the 30–50, 50–100, 100–300, and 300–600 keV energy bands. The average count rate is overplotted as a red dashed line, and a black solid line is overplotted at a count rate of 0 counts s^{-1}. The source was significantly detected in the first four energy bands at 1081.8σ, 770.6σ, 191.3σ, and 5.1σ. There was no detection in the highest-energy band (1.1σ). The coloring for the different revolutions is based on the spectral state analysis performed in Section 3.2.1.

3.1.2. 1E 1740.7–2942

1E is also a persistent source at hard X-ray/soft gamma rays, though it displays larger flux variability between observing periods with numerous times where the source count rate is marginally detected, or below the ISGRI detection limit. The ISGRI revolution timescale light curves are shown in Figure 2. As in the case of GRS, the 30–50, 50–100, 100–300, and 300–600 keV energy bands are plotted. 1E was significantly detected in the first four energy bands at 710.3σ, 467.3σ, 108.0σ, and 6.6σ, respectively, but it is not detected in the last energy channel (1.7σ). The coloring for the different

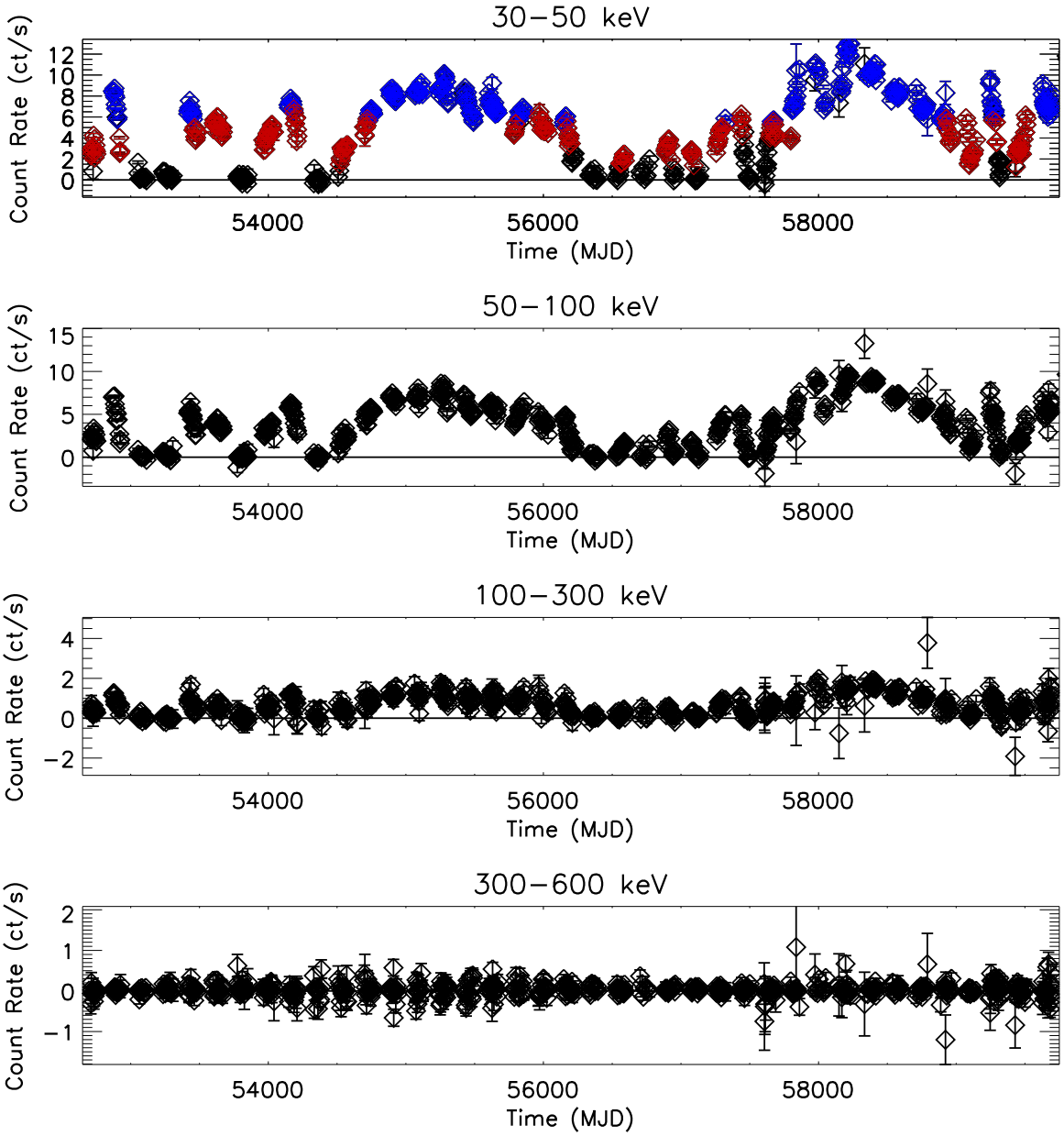

Figure 2. ISGRI long-term light curve of 1E in the 30–50, 50–100, 100–300, and 300–600 keV energy bands. Black solid line denotes 0 counts s^{-1}. The different colors in the 30–50 keV light curve correspond to different spectral states discussed in Section 3.2.2.

revolutions is based on the spectral state analysis performed in Section 3.2.2.

3.2. Spectral Variability

3.2.1. GRS 1758–258

To search for spectral variability, initially data were fit to a power-law model in the 30–90 keV energy range on a revolution timescale. However, the photon indexes were poorly constrained. Thus spectra from revolutions close in count rate and close in time were averaged to maximize statistics when fitting. The average photon indexes and the normalizations at 50 keV are plotted in Figure 3(a).

Though the normalization varies by a factor of roughly 7 (excluding the very low count-rate periods), the photon index does not show any clear correlation. For spectra with $\Gamma < 1.8$, the photon index is roughly constant at $\Gamma = 1.7$ for normalizations from $\sim 8 \times 10^{-5}$ to 2.8×10^{-4} ph cm^{-2} s^{-1}. These spectral parameters are shown as blue asterisks in Figure 3(a). At a normalization of approximately 3×10^{-4} ph cm^{-2} s^{-1}, the photon indices have values of roughly 1.7–1.8, which are plotted as red circles. These two spectral groupings are subsequently referred to as the "hard medium" and "hard high" states.

The vertical dashed line at $\Gamma = 1.8$ separates the "hard" and "soft" states. In contrast to the hard states, the soft states show a clearer relationship between photon index and normalization, with Γ decreasing as the normalization increases. The soft spectra were grouped into four normalization levels: below 1×10^{-4} ph cm^{-2} s^{-1} (soft low, plotted as black diamonds), 1×10^{-4} to 1.45×10^{-4} ph cm^{-2} s^{-1} (soft medium 1, plotted as green triangles), 1.45×10^{-4}–2.05×10^{-4} ph cm^{-2} s^{-1}

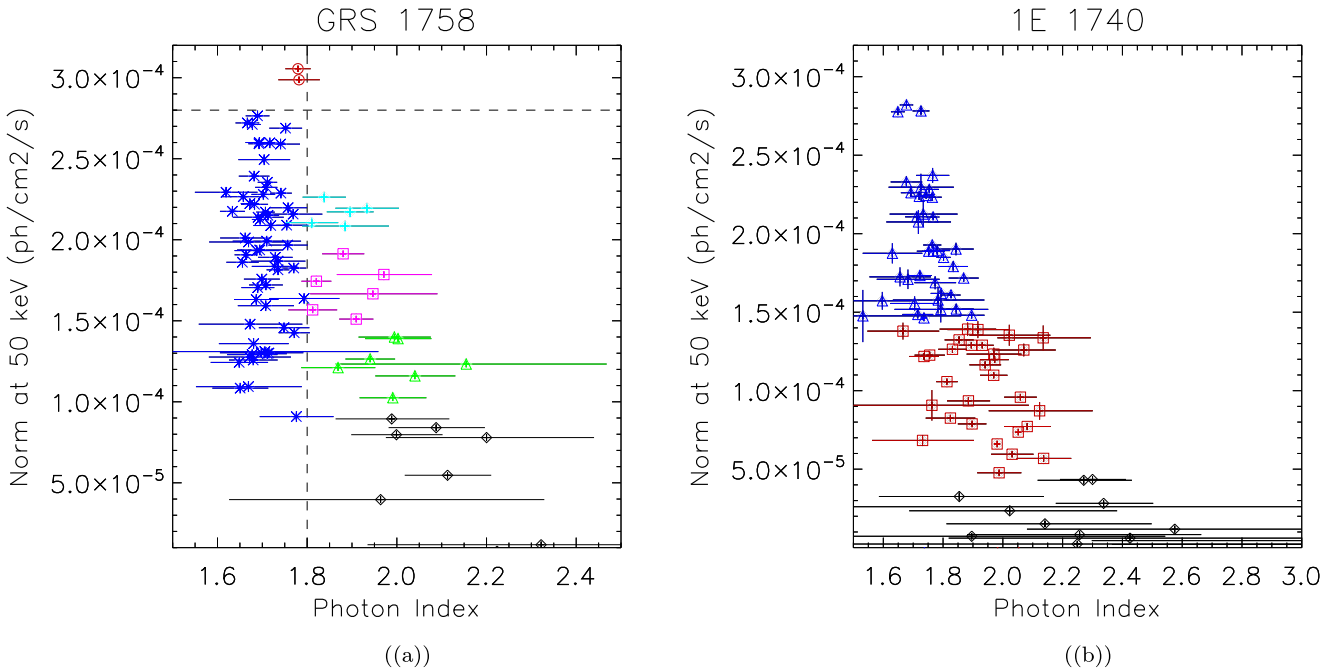

Figure 3. GRS and 1E photon index vs. 50 keV normalization for average spectral groups in panels (a) and (b), respectively. For GRS, the vertical dashed line at $\Gamma = 1.8$ marks the separation between the "hard" and "soft" groupings. For 1E, the low flux state corresponds to periods with normalization less than 4.5×10^{-5} ph cm^{-2} s^{-1}. The medium flux state corresponds to normalization between 4.5×10^{-5} and 1.45×10^{-4} ph cm^{-2} s^{-1}. The high flux state corresponds to normalization between above 1.45×10^{-4} ph cm^{-2} s^{-1}.

Table 1
Average Spectrum Parameters

GRS 1758–258									
	Power-Law		Cutoff Power-Law			CompTT			Exp. Time
	Γ	χ^2/ν	Γ	$E_{\rm cut}$ (keV)	χ^2/ν	kT_e (keV)	τ	χ^2/ν	(Ms)
Soft Low	2.06 ± 0.03	$35.50/27 = 1.31$	…	…	…	…	…	…	1.04
Soft Medium 1	1.93 ± 0.01	$43.87/27 = 1.32$	1.69 ± 0.06	242 ± 63	$28.14/26 = 1.08$	70 ± 68	0.7 ± 0.8	$28.89/26 = 1.11$	1.44
Soft Medium 2	1.97 ± 0.01	$78.98/27 = 2.93$	1.5 ± 0.08	139 ± 21	$28.68/26 = 1.10$	48 ± 8	1.1 ± 0.2	$30.68/26 = 1.18$	0.97
Soft High	1.95 ± 0.02	$90.58/27 = 3.36$	1.42 ± 0.08	110 ± 16	$35.18/27 = 1.35$	34 ± 3	1.5 ± 0.1	$31.72/26 = 1.22$	0.45
Hard Medium	1.739 ± 0.007	$359.14/27 = 13.19$	1.25 ± 0.03	137 ± 8	$51.80/26 = 1.99$	38.8 ± 1.0	1.73 ± 0.04	$21.49/26 = 0.83$	20.43
Hard High	1.8 ± 0.01	$90.58/32 = 3.36$	1.36 ± 0.09	120 ± 16	$25.38/26 = 0.98$	35 ± 2	1.6 ± 0.1	$22.51/26 = 0.87$	0.35

1E 1740.7–2942									
	Power-Law		Cutoff Power-Law			CompTT			Exp. Time
	Γ	χ^2/ν	Γ	$E_{\rm cut}$ (keV)	χ^2/ν	kT_e (keV)	τ	χ^2/ν	
Low	2.21 ± 0.07	$33.33/27 = 1.23$	…	…	…	…	…	…	4.55
Medium	1.953 ± 0.009	$115.49/27 = 4.28$	1.59 ± 0.04	168 ± 20	$34.29/26 = 1.32$	44 ± 4	1.2 ± 0.1	$27.97/26 = 1.04$	10.62
High	1.829 ± 0.007	$304.72/27 = 11.29$	1.32 ± 0.03	130 ± 8	$35.52/26 = 1.37$	38 ± 1	1.61 ± 0.05	$17.56/26 = 0.68$	10.83

(soft medium 2, plotted as magenta squares), and greater than 2.05×10^{-4} ph cm^{-2} s^{-1} (soft high, plotted as cyan plus signs).

The spectra within each spectral grouping were averaged together for six spectra. First, the spectra were fitted to a power law in the 30–150 keV energy range. The fit parameters for each spectrum are listed in Table 1. Only the soft low spectrum was acceptably described by a power law, which has a best-fit photon index of 2.06 ± 0.03. The residuals for the other spectra suggest the presence of a high-energy cutoff. Thus we fitted them using a cutoff power-law model (`cutoffpl`), and each spectrum is well described, though with significantly different

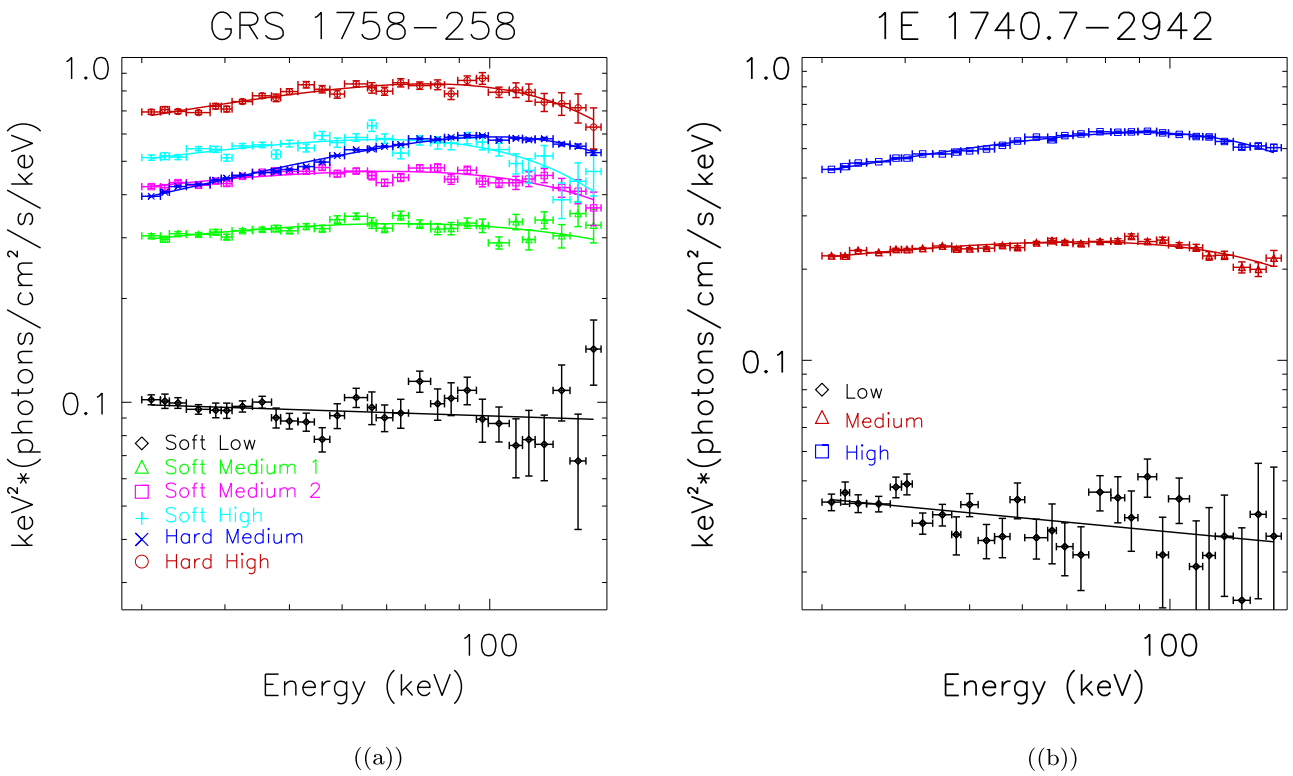

Figure 4. GRS (a) and 1E (b) average-state spectra in the 30–150 keV energy range with `CompTT` model fits overplotted for each spectrum, except for the low-state spectra, which are shown with power-law models.

Γ and cutoff energy ($E_{\rm cut}$) values. The soft medium 1, soft medium 2, and soft high spectra have decreasing photon indices from $\Gamma \sim 1.7$ to 1.4 and decreasing $E_{\rm cut}$ from ∼240 to 110 keV. The hard medium and hard high spectra show comparable photon indices (1.25 ± 0.03 and 1.36 ± 0.09, respectively) and cutoff energies (137 ± 8 keV and 120 ± 16 keV, respectively). However, the parameters are not acceptable for the hard medium spectrum ($\chi^2/\nu = 51.80/26 = 1.99$).

Subsequently, we fitted all the non-low-state spectra to the thermal Comptonization model `CompTT` assuming a disk accretion geometry. For each, the photon seed temperature (kT_0) was fixed to 0.5 keV. As with the cutoff power-law model, the electron temperature (kT_e) decreases as flux increases from ∼70 keV for the soft medium 1 spectrum to 34 keV for the soft high spectrum, though the medium 1 spectrum is poorly constrained (±68 keV). On the other hand, the optical depth (τ) increases as flux increases, going from 0.7 to 1.5. The hard spectra have similar kT_e values (38.8 and 35 for the medium and high spectra, respectively), but they have significantly different τ values (1.73 and 1.6 for the medium and high spectra, respectively). The average spectra with their `CompTT` model are plotted in Figure 4(a).

Due to the large amount of exposure time, and very stable instrumental background level, GRS is significantly detected above 150 keV in the hard medium state. Thus we extended the spectral fits up to 610 keV. For the `CompTT` model kT_e is 44.0 ± 0.8 keV, larger than the fit up to 150 keV, and τ decreases from 1.73 to 1.54 ($\chi^2/\nu = 61.90/36 = 1.72$). The fit parameters for this model and subsequent models are listed in Table 2. However, above ∼200 keV the residuals are all above the model, suggesting the presence of a possible high-energy component. Therefore we added a power-law model to fit the spectrum above 200 keV. The χ^2/ν improved to $36.82/34 = 1.08$ with $kT_e = 36$ keV, $\tau = 1.9$, and $\Gamma = 1.8$. Thus a high-energy component is needed to acceptably fit the spectrum above 150 keV. To test the significance of the power-law component, we performed an F-test and found an F-statistic of 17.62 and probability of 5.61×10^{-6} (∼4.5σ). The spectrum with the `CompTT+powerlaw` model is plotted in Figure 5 as black diamonds. The medium and high spectra for 1E are also shown as red squares and blue triangles, respectively.

Similar high-energy excesses have been observed in other accreting black holes (e.g., GX 339–4, W. N. Johnson et al. 1993; Cyg X-1, M. L. McConnell et al. 2000; GRS 1915+105, A. A. Zdziarski et al. 2001), which has largely been confirmed with INTEGRAL (see S. E. Motta et al. 2021). The origin of the emission is debated. Polarization results of the high-energy spectrum of Cyg X-1 from INTEGRAL (P. Laurent et al. 2011; E. Jourdain et al. 2012) suggest that the emission is associated with the jet that is observed at radio wavelengths. However, the excess can also be explained by a hybrid thermal/nonthermal population of electrons in the corona (P. S. Coppi 1999). Thus we fit the spectrum to the `Eqpair` model. Following M. Gierliński et al. (1999), M. Del Santo et al. (2008), and T. Bassi et al. (2020), we left the l_h/l_s (the ratio of the hard to soft compactness), l_{nt}/l_n (the fraction of power going to the energetic particles that accelerates the nonthermal particles), and τ_p (the Thomson scattering depth) parameters free while l_{bb} (the soft photon compactness) was fixed to 10 and $G_{\rm inj}$ (the index of the electron distribution) was fixed to 2.5. Additionally, kT_{bb} (the temperature of the inner edge of the accretion disk) was fixed to 0.5 keV, and the ionization parameter of the reflector (ξ) and the reflection fraction were fixed to 0. The best-fit parameters are $l_h/l_s = 6.7 \pm 0.1$, $l_{nt}/l_h = 0.58 \pm 0.07$,

Table 2
30–610 keV Fit Spectral Parameters

	CompTT			CompTT+po				Eqpair			
	kT_e (keV)	τ	χ^2/ν	kT_e (keV)	τ	Γ	χ^2/ν	l_h/l_s	l_{nt}/l_h	τ_p	χ^2/ν
GRS 1758–258											
Medium	44.0 ± 0.8	1.54 ± 0.08	61.90/36 = 1.72	36 ± 3	1.9 ± 0.3	1.8 ± 0.2	36.82/34 = 1.08	6.7 ± 0.1	0.58 ± 0.07	1.1 ± 0.2	30.05/35 = 0.86
1E 1740.7–2942											
Medium	57 ± 6	0.9 ± 0.1	45.13/36 = 1.25	35 ± 6	1.3 ± 0.2	1.3 ± 1.0	33.37/34 = 0.98	3.8 ± 0.2	0.84 ± 0.08	1.2 ± 0.1	30.35/35 = 0.87
High	43 ± 4	1.44 ± 0.04	68.67/36 = 1.91	34 ± 4	1.7 ± 0.3	1.5 ± 0.8	33.72/34 = 0.99	5.9 ± 0.2	0.87 ± 0.09	1.1 ± 0.2	31.36/35 = 0.90

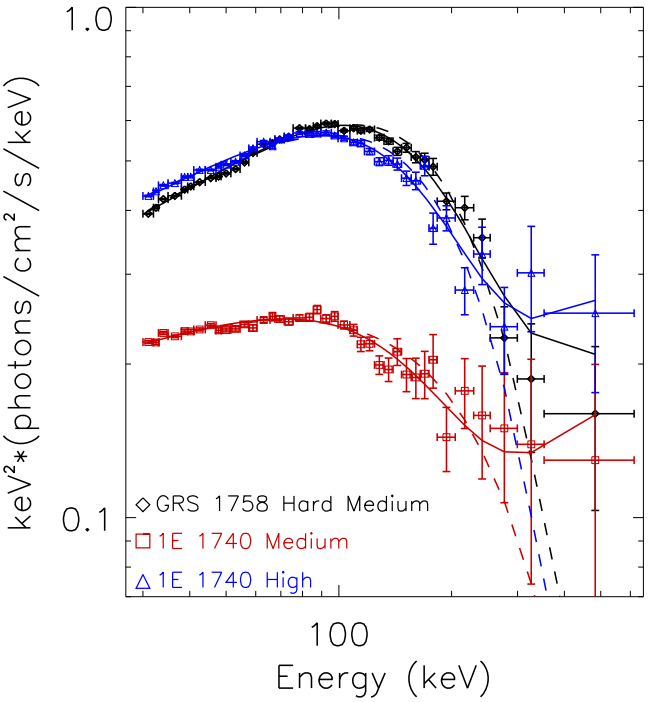

Figure 5. Average-state spectra for GRS hard medium (black diamonds) and 1E medium (red squares) and high (blue triangles) in the 30–610 keV energy range. The CompTT+powerlaw model is overplotted as a solid line for each, while the CompTT model is overplotted as a dashed line.

and $\tau_p = 1.1 \pm 0.2$ with $\chi^2/\nu = 30.05/35 = 0.86$. Thus the model also well describes the data.

3.2.2. 1E 1740.7–2942

The same search for spectral variability was performed for 1E. Figure 3(b) shows the photon index and normalization behavior. In contrast to GRS, 1E exhibits a more straightforward relationship between the 50 keV flux and photon index. Groupings with normalizations below 4.5×10^{-5} ph cm^{-2} s^{-1} (low state, plotted as black diamonds) have $\Gamma \sim 2.2$, though many of the photon indices are poorly constrained. For normalizations from 4.5×10^{-5} to 1.45×10^{-4} ph cm^{-2} s^{-1} (medium state, plotted as red squares), groupings have an average Γ of roughly 1.9. Finally, the high state groupings ($>1.45 \times 10^{-4}$ ph cm^{-2} s^{-1}, plotted as blue triangles) have an average photon index of approximately 1.75.

As with GRS, we averaged the spectral groupings together and fitted them with a power-law model. Again, the low flux state is consistent with a power law $\Gamma = 2.21 \pm 0.07$, while the medium- and high-flux-state spectra are suggestive of a high-energy cutoff. The fit parameters for all the models are shown in Table 1. We fitted the medium and high spectra to a cutoff power-law model. The medium spectrum fit improves but is still not acceptable ($\chi^2/\nu = 34.29/26 = 1.32$) for $\Gamma = 1.59 \pm 0.04$ and $E_{\rm cut} = 168 \pm 20$ keV. Also, the χ^2/ν for the high state is still unacceptable ($35.52/26 = 1.37$) with $\Gamma = 1.32 \pm 0.03$ and $E_{\rm cut} = 130 \pm 8$ keV.

Next, we fitted both spectra to a CompTT model. In this case, the model describes the data well $\chi^2/\nu = 27.97/26 = 1.04$ for the medium state and $17.56/26 = 0.68$ for the high state. The medium spectrum has a kT_e of 44 keV and τ of 1.2 compared to kT_e of 38 keV and τ of 1.61 for the high spectrum.

The medium and high flux spectra show significant emission above 150 keV. Thus we again investigated the presence of a high-energy tail by fitting the spectrum up to 610 keV. For the medium spectrum, the CompTT fit has an increased kT_e from 44 to 57 keV and a decreasing τ from 1.2 to 0.9. The χ^2/ν is acceptable (1.25), but again the high-energy residuals are all above the model and suggest the presence of an additional spectral component. The fit parameters are listed for this fit and subsequent fits in Table 2. Including a power-law at high energies with $\Gamma = 1.3$ reduces the electron temperature (35 keV) and increases the optical depth (1.3) and reduces the χ^2 to 33.37 for $\nu = 34$ ($\chi^2/\nu = 0.98$). Results of an F-test found an F-statistic of 5.99 and probability of 0.0059 ($\sim 2.8\sigma$), and thus the additional component is not significant.

Nonetheless, we fitted the spectrum with the Eqpair model. The fit parameters are $l_h/l_s = 3.8 \pm 0.2$, $l_{nt}/l_h = 0.84 \pm 0.08$, and $\tau_p = 1.2 \pm 0.1$ with $\chi^2/\nu = 30.35/35 = 0.87$. The τ_p values are similar to GRS, while the l_nt/l_h and l_h/l_s are significantly different (3.8 compared to 6.7 and 0.58 compared to 0.84, respectively).

We performed the same analysis for the high state. In this case the CompTT model is a poor fit to the model ($\chi^2/\nu = 68.67/36 = 1.91$) due to the excess at high energies. Adding a power-law component significantly improves the quality of the fit ($\chi^2/\nu = 33.72/34 = 0.99$) with $kT_e = 34$ keV, $\tau = 1.7$, and $\Gamma = 1.5$. An F-test analysis finds an F-statistic of 17.62 and a probability of 5.61×10^{-6} ($\sim 4.5\sigma$). An Eqpair model fit also

acceptably fits the data ($\chi^2/\nu = 31.36/35 = 0.90$) with $l_h/l_s = 5.9 \pm 0.2$, $l_{nt}/l_h = 0.87 \pm 0.09$, and $\tau_p = 1.1 \pm 0.2$. The τ_p values are comparable to GRS 1758, but l_{nt}/l_h is significantly higher. The l_h/l_s value of GRS is higher than both those for 1E. As before, the medium and high spectra are also shown as red squares and blue triangles, respectively, in Figure 5.

4. Discussion

4.1. Comparison with Previous Works

4.1.1. GRS 1758–258

There have been several works studying the long-term behavior of GRS up to roughly a couple of hundred keV to compare with our INTEGRAL observations. GRANAT/SIGMA monitored GRS (and 1E) in the 40–200 keV energy range from 1990 to 1998. S. I. Kuznetsov et al. (1999) found cutoff spectral parameters of $\Gamma = 1.0 \pm 0.3$ and $E_{\rm cut} = 89^{+40}_{-20}$ keV and `CompTT` parameters of $kT_e = 41^{+7}_{-5}$ keV and $\tau = 1.2 \pm 0.2$. These values are most similar to the 30–150 keV hard medium spectrum. Γ and kT_e are comparable to the ISGRI values ($\Gamma = 1.25$ and $kT_e = 38.8$ keV), but the $E_{\rm cut}$ and τ values are significantly different (137 keV and 1.73), suggesting that the spectral curvature in the SIGMA spectrum is different from the ISGRI one.

BeppoSAX observed GRS on 1997 April 10–11, in the 0.1–200 keV energy range. The continuum spectrum was well described by an absorbed power law with a high-energy cutoff (`powerlaw*highecut`) with $\Gamma = 1.65$, $E_{\rm cut} = 73$ keV, and $E_{\rm fold} = 180$ keV (L. Sidoli & S. Mereghetti 2002). We fitted our hard medium spectrum with the same model without the low-energy absorption in the 30–210 keV energy range and found comparable parameters ($\Gamma = 1.60$, $E_{\rm cut} = 85$ keV, and $E_{\rm fold} = 185$ keV). The authors also fit the spectrum to a `CompTT` model but assuming a spherical accretion geometry. Thus we refitted the hard medium spectrum using the same assumption. Again, the fit resulted in similar parameters (ISGRI: $kT_e = 42$ keV, $\tau = 3.8$ and BeppoSAX: $kT_e = 44$ keV, $\tau = 3.6$).

K. Pottschmidt et al. (2008) analyzed the INTEGRAL/SPectrometer on INTEGRAL (SPI) and IBIS data from early in the mission (2003–2007) and reported the presence of a hard tail above ∼300 keV. Their best-fit `CompTT+po` model had $kT_e = 41$ keV, $\tau = 1.4$, and $\Gamma = 1.4$, though they found that it is possible to get an equally good fit with $\Gamma = 2.0$, comparable to the photon index that we report (1.8). However, we tested our spectrum with $\Gamma = 1.4$, and the fit is comparable ($38.56/35 = 1.10$ versus $36.82/34 = 1.08$) with $kT_e = 38$ keV and $\tau = 1.70$.

4.1.2. 1E 1740.7–2942

As mentioned in the previous section, SIGMA observed 1E from 1990–1998. Its average spectrum was well fit by a cutoff spectrum with $\Gamma = 1.2 \pm 0.02$ and $E_{\rm cut} = 110^{+26}_{-23}$ keV (S. I. Kuznetsov et al. 1999), similar to the high-state spectrum ($\Gamma = 1.32$, $E_{\rm cut} = 130$ keV), though with a lower Γ. For the `CompTT` fit, the kT_e values are not similar (44 keV for SIGMA and 35 keV for ISGRI), while the optical depths are (1.63 compared to 1.60 for SIGMA and ISGRI, respectively). Thus it is unclear which spectral state the SIGMA observations correspond to compared to the ISGRI spectrum.

L. Bouchet et al. (2009) analyzed the ISGRI and INTEGRAL/SPI observations from 2003 to 2005 in the 18–600 keV energy range. They found a significant excess above 200 keV. Thus their spectrum more closely matches our high-state spectrum, which has a similar 30 keV flux. Including a power law for the high-energy component to the `CompTT` model resulted in an acceptable fit with $kT_e = 27 \pm 2.2$ keV, $\tau = 1.9 \pm 0.25$, and $\Gamma = 1.9 \pm 0.1$ compared to ($kT_e = 35 \pm 6$ keV, $\tau = 1.3 \pm 0.2$, $\Gamma = 1.3 \pm 1.0$) for our spectrum. Fixing kT_e and Γ to the values from L. Bouchet et al. (2009), we find $\tau = 2.56 \pm 0.03$, significantly higher.

They also tested a scenario where the high-energy emission is due to a second thermal Comptonization component for a `CompTT+CompTT` model with best-fit parameters $kT_{e_1} = 29.4 \pm 3.1$ keV, $\tau_1 = 1.6 \pm 0.1$, $kT_{e_2} = 100$ keV (fixed), and $\tau_2 = 2.2 \pm 0.8$. The seed photon temperature for the second `CompTT` component was tied to kT_{e_1}. We fitted our spectrum to this scenario with comparable parameters for the `CompTT` component ($kT_{e_1} = 25 \pm 3$ keV and $\tau = 1.77 \pm 0.06$), but the optical depth for the second component is significantly different (1.0 ± 0.3).

4.2. Origin of the High-energy Emission

As mentioned above, the physical mechanism that produces the high-energy excess, or hard tail, remains unclear. A possible explanation is that the photons are produced by a hybrid thermal/nonthermal Comptonizing plasma (P. S. Coppi 1999). This model has been used to explain the hard tails in Cyg X-1 in the soft state (M. Gierliński et al. 1999; F. Cangemi et al. 2021), GX 339–4 (M. Del Santo et al. 2008), and GRS 1716–249 (T. Bassi et al. 2020), among other sources.

Another suggested interpretation is that the hard tail is due to a second thermal Comptonizing component. L. Bouchet et al. (2009) applied this interpretation to 1E, as seen in the previous section.

A third possibility is that the excess is nonthermal emission related to the radio jet. Observations since the early 2000s have found steady, compact jets in radio observations of numerous black hole binaries in the hard state (R. Fender & T. Belloni 2004). During the soft state, the jet is either not present or extremely faint (T. D. Russell et al. 2019; T. J. Maccarone et al. 2020). During the hard to soft state transition, the jet becomes unstable and flares are seen at radio wavelengths (R. Fender (2006) and references within. Polarization detections by INTEGRAL of Cyg X-1 (P. Laurent et al. 2011; E. Jourdain et al. 2012), MAXI J1348–630 (F. Cangemi et al. 2023), and Swift J1727.8–1613 (T. Bouchet et al. 2024) support this interpretation, at least in some sources.

GRS and 1E radio observations have long reported the existence of persistent jets (e.g., L. F. Rodriguez et al. 1992; I. F. Mirabel & L. F. Rodríguez 1999; J. Martí et al. 2017; A. J. Tetarenko et al. 2020). A study of the spectral states in GRS with RXTE/PCA and the Very Large Array during 2001–2003 found behavior consistent with the standard hard/soft paradigm R. Soria et al. (2011) presented above. For 1E, multiwavelength analysis during 2007 July shows only the upper limits from ATCA observations during a soft state (J. M. Dickey et al. 2023), suggesting that 1E also follows the expected behavior.

In the jet interpretation, the soft gamma-ray photons are produced at the base of the jet (A. A. Zdziarski 2012). In

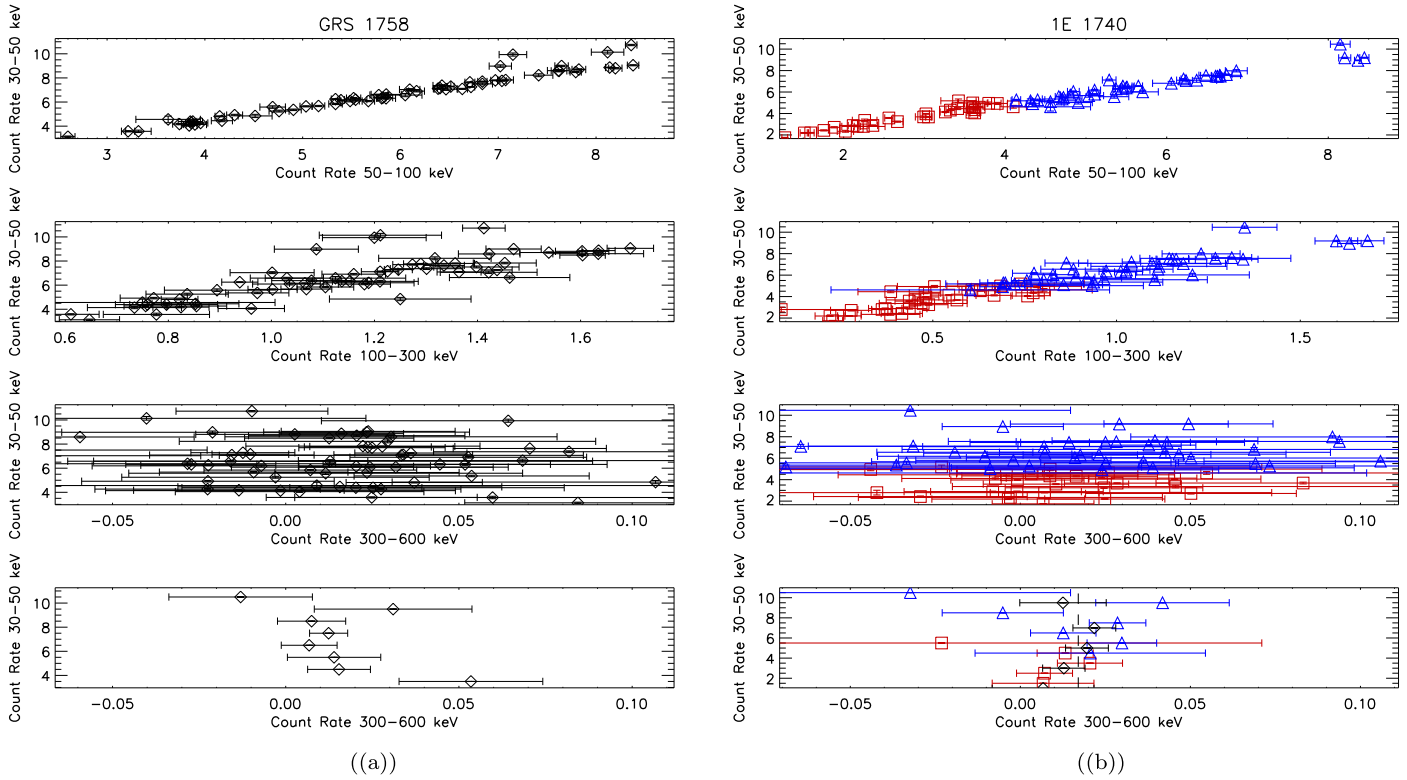

Figure 6. The 50–100 keV (first), 100–300 keV (second), and 300–600 (third and fourth) keV count rates vs. 30–50 keV count rate for the GRS hard medium state (a) and the 1E medium and high states (b), which are plotted as red squares and blue triangles, respectively. The bottom panel shows the 300–600 vs. 30–50 keV count rates with the data rebinned in 1 count s^{-1} bins and the 2 counts s^{-1} bins plotted as black diamonds with the best-fit constant value overplotted as a black dotted line.

contrast, the emission is connected to the corona in the hybrid thermal/nonthermal plasma and second thermal Comptonizing component interpretations. In the hybrid thermal/nonthermal model, the thermal and nonthermal electrons come from the accretion flow (J. Poutanen & A. Veledina 2014). The nonthermal electrons are possibly produced by shock acceleration (P. C. Fragile & O. M. Blaes 2008; S. Das et al. 2009; K. B. Henisey et al. 2012) or magnetic reconnection (J. Ding et al. 2010; M. A. Riquelme et al. 2012; M. Hoshino 2013). Thus any changes in the accretion flow that affect the population of thermal electrons are expected to also affect the nonthermal electron population, resulting in a correlation between the two components. Thus a possible way to differentiate between the corona and jet interpretations is to investigate the correlations between the hard X-rays and the soft gamma rays.

Therefore, we looked for correlations in count rates between four broad energy bands in the GRS hard medium state and the 1E medium and high states. Figure 6(a) shows the 30–50 keV count rate versus the 50–100 keV count rate (first panel), 100–300 keV (second panel), and 300–600 keV (third and fourth panels). The bottom panels show the same data as the third panel, but the data were rebinned to 1 count s^{-1} bins. Figure 6(b) shows the same plots for 1E with the medium state plotted as red squares and the high state plotted as blue triangles. For each panel, we calculated the Spearman correlation coefficient and the standard deviation from a null correlation.

In the case of GRS, the Spearman coefficients (and standard deviations) are 0.98 (−7.63), 0.86 (−6.65), and −0.07 (0.58) for the 50–100, 100–300, and 300–600 keV energy bands, respectively. There are strong correlations between the 30–50 keV band count rate and the count rates in the next two higher-energy bands. However, there is no strong correlation between the 30–50 keV and 300–600 keV count rates. The lack of correlation may be due to large errors in the 300–600 keV count rates, so we rebinned the data in 1 count s^{-1} bins based on the 30–50 keV count rate. Even with higher statistics, there is still no significant correlation between the two energy bands with a coefficient of −0.57 (1.51), though there is a weak anticorrelation between the two energy bands, which is biased by the highest and lowest count-rate points. If they are excluded, the coefficient (and standard deviation) are 0.02 (−0.06).

For 1E, the medium state correlations (and standard deviations) are 0.92 (−4.96), 0.84 (−4.51), and −0.04 (0.23) for the 50–100, 100–300, and 300–600 keV energy bands, respectively. For the high state, the values are 0.95 (−5.84), 0.85 (−5.27), and 0.21 (−1.27) for the same energy bands as the medium state. Thus in both states there are strong correlations between the 30–50 keV count rates and the count rates in the next two higher bands, but no significant correlation between the 300–600 keV count rates. Again, the 300–600 keV count rates are low, so we rebinned the data as was done for GRS and calculated the correlations (and standard deviations). There is still no strong correlation with coefficients of −0.10 (0.20) and −0.29 (0.70) for the medium and high states, respectively. The scatter between the points was still large, so we combined the data in 2 counts s^{-1} bins and across spectral states (shown in the bottom panel with black diamonds). In this case, there is a weak positive correlation of 0.40 (−0.80). As with GRS, the lowest and highest count-rate values heavily influence the results. Excluding the lowest point, the correlation is −0.20 (0.35), while excluding the highest point the

correlation is 1.00 (−1.73). However, the 300–600 count rates are consistent with a constant value of 0.017 ± 0.003 counts s^{-1} ($\chi^2/\nu = 1.79/4 = 0.45$), which is plotted as a black dashed line in the bottom panel of Figure 6(b).

The strong correlation between the count rates below 300 keV suggests that those photons originate from the same mechanism. This is consistent with the spectral fitting, which finds that thermal Comptonization dominates up to ∼200 keV. However, a lack of strong correlation between the hard X-rays (30–50 keV) and the soft gamma rays (300–600 keV) suggests that the high-energy photons arise from a different mechanism. These results then favor the jet interpretation over the corona interpretation for the origin of the high-energy excess in GRS. For 1E, the interpretation is less clear. The results when rebinning in 2 counts s^{-1} intervals are suggestive of a correlation when including all the points (0.40), but the correlation coefficient is heavily dependent on the lowest count-rate value, and the count rates are consistent with a constant value. Detections of polarization in the sources could help determine the origin of the hard tails. However, the 300–600 keV fluxes for the sources are quite low compared to previous sources with polarization detections from IBIS or SPI. The GRS hard medium flux is roughly 50 mCrab compared to the Crab spectrum reported in E. Jourdain & J. P. Roques (2020). The 1E medium and high fluxes are approximately 33 and 60 mCrab, respectively. The hard-tail fluxes are roughly 1 order of magnitude lower than those of Cyg X-1 (P. Laurent et al. 2011), making the detection of polarization difficult (S. E. Motta et al. 2021).

5. Conclusion

INTEGRAL's extensive monitoring of GRS and 1E for over 20 yr has enabled an in-depth study of the spectral behavior of the two sources from hard X-rays to soft gamma rays, and we investigated their characteristics up to 600 keV. In the case of GRS, we found it to be predominately in a spectral state with a Comptonized spectrum that does not vary with flux (∼20/25 Ms). For comparatively brief periods during our observations, the source displayed a flux-dependent spectral behavior where the 30–90 keV photon index decreased as the 50 keV flux increased. In contrast, 1E exhibited a more straightforward spectral–flux relationship where the 30–90 keV spectrum hardens as the 50 keV flux increases, though the spectrum is relatively stable in the flux ranges: $<4.5 \times 10^{-5}$ ph cm^{-2} s^{-1}, 4.5×10^{-5}–1.45×10^{-4} ph cm^{-2} s^{-1}, $>1.45 \times 10^{-4}$ ph cm^{-2} s^{-1}.

Three of the spectra showed significant emission up to ∼600 keV (GRS hard medium, 1E medium and high). Subsequently, we fitted the 30–610 keV energy range to a `CompTT` model. The residuals of each spectrum showed an excess above roughly 200 keV. For the GRS hard medium and 1E high-state spectra the χ^2/ν values are unacceptable, while the fit to the 1E medium state is still acceptable. The residuals in each fit showed an excess above ∼200 keV. Thus we fitted the spectra with a `CompTT+powerlaw` model. The χ^2/ν improves in each case, but the improvement was not significant for the 1E medium state (∼2.8σ). For the GRS hard medium and 1E high state, the fits become acceptable ($\chi^2/\nu = 1.08$ and $= 0.99$, respectively).

As the nature of the high-energy excess remains unclear, we tested a scenario where those photons are from a hybrid thermal/nonthermal corona using the `Eqpair` model. In each fit, the fraction of power devoted to energetic particles accelerating the nonthermal particles is >0.58 and statistically significant (>8σ), supporting the presence of a high-energy excess in each spectrum.

However, the hard tails may also be associated with the radio jet, as has been reported for Cyg X-1, MAXI J1348–630, and Swift J1728.8–1613, based on polarization measurements. To differentiate between the two scenarios, we investigated the energy-dependent correlations for each. We found that the 30–50 keV count rates are strongly correlated with the count rates below 300 keV. However, above 300 keV the behavior changes. For GRS and the 1E medium and hard states there are weak anticorrelations (−0.57, −0.10, and −0.29, respectively) between the 30–50 keV and 300–600 keV energy bands when rebinning the data for higher statistics.

The lack of a positive correlation between the 30–50 keV and 300–600 keV count rates suggests that photons for the two energy bands are produced in different locations, or by different physical processes, which would be in tension with the hybrid thermal/nonthermal Comptonization scenario. Thus these results seem to support a jet origin for the high-energy photons, at least in the case of GRS, but due to the low count rate in the 300–600 keV energy band, the anticorrelations and lack of correlation are not significant enough to exclude the possibility of a positive correlation. For 1E, the interpretation is more complicated due to the large scatter in the 300–600 keV count rates, even when rebinned. Further rebinning results in a positive, but weak, correlation, though with few bins and combining different spectral states. However, the 300–600 keV count rate is consistent with a constant value, supporting a jet origin interpretation, but not excluding a corona origin interpretation.

Acknowledgments

The authors thank the referee for comments and suggestions to improve the paper. The authors thank the Italian Space Agency for the financial support under the "INTEGRAL ASI-INAF" agreement No. 2019-35-HH.0. The research leading to these results has received funding from the European Union's Horizon 2020 Programme under the AHEAD2020 project (grant agreement No. 871158). Based on observations with INTEGRAL, an ESA project with instruments and science data center funded by ESA member states (especially the PI countries: Denmark, France, Germany, Italy, Switzerland, Spain) and with the participation of Russia and the USA.

ORCID iDs

James Rodi https://orcid.org/0000-0003-2126-5908
Angela Bazzano https://orcid.org/0000-0002-2017-4396
Pietro Ubertini https://orcid.org/0000-0003-0601-0261

References

Bassi, T., Malzac, J., Del Santo, M., et al. 2020, MNRAS, 494, 571
Bouchet, L., Del Santo, M., Jourdain, E., et al. 2009, ApJ, 693, 1871
Bouchet, T., Rodriguez, J., Cangemi, F., et al. 2024, A&A, 688, L5
Cangemi, F., Beuchert, T., Siegert, T., et al. 2021, A&A, 650, A93
Cangemi, F., Rodriguez, J., Belloni, T., et al. 2023, A&A, 669, A65
Castro, M., D'Amico, F., Braga, J., et al. 2014, A&A, 569, A82
Coppi, P. S. 1999, in ASP Conf. Ser. 161, High Energy Processes in Accreting Black Holes, ed. J. Poutanen & R. Svensson (San Francisco, CA: ASP), 375
Das, S., Becker, P. A., & Le, T. 2009, ApJ, 702, 649
Del Santo, M., Bazzano, A., Zdziarski, A. A., et al. 2005, A&A, 433, 613
Del Santo, M., Malzac, J., Jourdain, E., et al. 2008, MNRAS, 390, 227
Dickey, J. M., Vrtilek, S. D., McCollough, M., et al. 2023, ApJS, 268, 35

Ding, J., Yuan, F., & Liang, E. 2010, ApJ, 708, 1545
Fender, R. 2006, in Compact Stellar X-ray Sources, ed. W. Lewin & M. van der Klis (Cambridge: Cambridge Univ. Press), 381
Fender, R., & Belloni, T. 2004, ARA&A, 42, 317
Fragile, P. C., & Blaes, O. M. 2008, ApJ, 687, 757
Gierliński, M., Zdziarski, A. A., Poutanen, J., et al. 1999, MNRAS, 309, 496
Henisey, K. B., Blaes, O. M., & Fragile, P. C. 2012, ApJ, 761, 18
Hoshino, M. 2013, ApJ, 773, 118
Jensen, P. L., Clausen, K., Cassi, C., et al. 2003, A&A, 411, L7
Johnson, W. N., Kurfess, J. D., Purcell, W. R., et al. 1993, A&AS, 97, 21
Jourdain, E., & Roques, J. P. 2020, ApJ, 899, 131
Jourdain, E., Roques, J. P., Chauvin, M., & Clark, D. J. 2012, ApJ, 761, 27J
Kuznetsov, S. I., Gilfanov, M. R., Churazov, E. M., et al. 1999, AstL, 25, 351
Laurent, P., Rodriguez, J., Wilms, J., et al. 2011, Sci, 332, 438L
Lebrun, F., Leray, J. P., Lavocat, P., et al. 2003, A&A, 411, L141
Maccarone, T. J., Osler, A., Miller-Jones, J. C. A., et al. 2020, MNRAS, 498, L40
Martí, J., Luque-Escamilla, P. L., Bosch-Ramon, V., et al. 2017, NatCo, 8, 1757
McConnell, M. L., Ryan, J. M., Collmar, W., et al. 2000, ApJ, 543, 928
Mirabel, I. F., & Rodríguez, L. F. 1999, ARA&A, 37, 409
Motta, S. E., Rodriguez, J., Jourdain, E., et al. 2021, NewAR, 93, 101618
Natalucci, L., Tomsick, J. A., Bazzano, A., et al. 2014, ApJ, 780, 63
Pottschmidt, K., Chernyakova, M., Lubiński, P., et al. 2008, in Proc. 7th INTEGRAL Workshop, 98
Pottschmidt, K., Chernyakova, M., Zdziarski, A. A., et al. 2006, A&A, 452, 285
Poutanen, J., & Veledina, A. 2014, SSRv, 183, 61
Riquelme, M. A., Quataert, E., Sharma, P., et al. 2012, ApJ, 755, 50
Rodriguez, L. F., Mirabel, I. F., & Marti, J. 1992, ApJL, 401, L15
Russell, T. D., Tetarenko, A. J., Miller-Jones, J. C. A., et al. 2019, ApJ, 883, 198
Sidoli, L., & Mereghetti, S. 2002, A&A, 388, 293
Soria, R., Broderick, J. W., Hao, J., et al. 2011, MNRAS, 415, 410
Tetarenko, A. J., Rosolowsky, E. W., Miller-Jones, J. C. A., et al. 2020, MNRAS, 497, 3504
Ubertini, P., Lebrun, F., Di Cocco, G., et al. 2003, A&A, 411, L131
Zdziarski, A. A. 2012, MNRAS, 422, 1750
Zdziarski, A. A., Grove, J. E., Poutanen, J., et al. 2001, ApJL, 554, L45